International Journal of Nanomedicine

Dovepress
open access to scientific and medical research

Open Access Full Text Article

ORIGINAL RESEARCH

Pycnoporus sanguineus Polysaccharides as Reducing Agents: Self-Assembled Composite Nanoparticles for Integrative Diabetic Wound Therapy

Xiaofei Huang[1], Lihua Shi[1], Yin Lin[1], Cong Zhang[1], Penghui Liu[1], Ran Zhang[2], Qiqi Chen[1], Xudong Ouyang[3], Yuanyuan Gao[2], Yingshuai Wang[3,*], Tongyi Sun[1,*]

[1]Shandong Key Laboratory of Proteins and Peptides Pharmaceutical Engineering, Shandong Universities Key Laboratory of Biological Medicine, School of Life Science and Technology, Weifang Medical University, Weifang, Shandong, 261053, People's Republic of China; [2]School of Pharmacy, Weifang Medical University, Weifang, Shandong, 261053, People's Republic of China; [3]School of Life Science and Technology, Weifang Medical University, Weifang, Shandong, 261053, People's Republic of China

*These authors contributed equally to this work

Correspondence: Tongyi Sun, Shandong Key Laboratory of Proteins and Peptides Pharmaceutical Engineering, Shandong Universities Key Laboratory of Biological Medicine, School of Life Science and Technology, Weifang Medical University, Baotong Road, Weifang, Shandong, 261053, People's Republic of China, Tel/Fax +86-536-8462067, Email sd_sty@126.com; Yingshuai Wang, School of Life Science and Technology, Weifang Medical University, Baotong Road, Weifang, Shandong, 261053, People's Republic of China, Tel/Fax +86-536-8462052, Email yingshuaiwang1987@163.com

Purpose: Diabetic foot ulcers (DFU) are severe complications of diabetes, posing significant health and societal challenges. Elevated levels of reactive oxygen species (ROS) at the ulcer site hinder wound healing in most patients, while individuals with diabetes are also more susceptible to bacterial infections. This study aims to synthesize a comprehensive therapeutic material using polysaccharides from *Pycnoporus sanguineus* to promote DFU wound healing, reduce ROS levels, and minimize bacterial infections.

Methods: Polysaccharides from *P.sanguineus* were employed as reducing and stabilizing agents to fabricate polysaccharide-based composite particles (PCPs) utilizing silver ions as templates. PCPs were characterized via UV-Vis, TEM, FTIR, XRD, and DLS. The antioxidant, antimicrobial, and cytotoxic properties of PCPs were assessed through in vitro and cellular experiments. The effects and mechanisms of PCPs on wound healing were evaluated using a diabetic ulcer mouse model.

Results: PCPs exhibited spherical particles with an average size of 57.29±22.41 nm and effectively combined polysaccharides' antioxidant capacity with silver nanoparticles' antimicrobial function, showcasing synergistic therapeutic effects. In vitro and cellular experiments demonstrated that PCPs reduced cellular ROS levels by 54% at a concentration of 31.25 μg/mL and displayed potent antibacterial activity at 8 μg/mL. In vivo experiments revealed that PCPs enhanced the activities of superoxide dismutase (SOD) and catalase (CAT), promoting wound healing in DFUs and lowering the risk of bacterial infections.

Conclusion: The synthesized PCPs offer a novel strategy for the comprehensive treatment of DFU. By integrating antioxidant and antimicrobial functions, PCPs effectively promote wound healing and alleviate patient suffering. The present study demonstrates a new strategy for the integrated treatment of diabetic wounds and expands the way for developing and applying the polysaccharide properties of *P. sanguineus*.

Keywords: *Pycnoporus sanguineus*, polysaccharide, injury, antioxidant, antibacterial

Introduction

Diabetic foot ulcer (DFU) is a common chronic complication of diabetes with high morbidity that leads to amputation, disability and death.[1] Oxidative stress and persistent wound infection are the two most important causes of wound healing in diabetic ulcers.[2,3] The high Reactive Oxygen Species (ROS) level at the wound site makes wounds difficult to heal.[4] Meanwhile, open high glucose wounds are more susceptible to bacterial infection and promote bacterial proliferation,[5] leading to the formation of biofilms, which can affect drug penetration and inhibit self-healing.[6] Clearance of bacterial infection is beneficial for wound healing. However, the bacterial infection also stimulates the

Received: 19 July 2023
Accepted: 10 October 2023
Published: 26 October 2023

© 2023 Huang et al. This work is published and licensed by Dove Medical Press Limited. The full terms of this license are available at https://www.dovepress.com/terms.php and incorporate the Creative Commons Attribution – Non Commercial (unported, v3.0) License (http://creativecommons.org/licenses/by-nc/3.0/). By accessing the work you hereby accept the Terms. Non-commercial uses of the work are permitted without any further permission from Dove Medical Press Limited, provided the work is properly attributed. For permission for commercial use of this work, please see paragraphs 4.2 and 5 of our Terms (https://www.dovepress.com/terms.php).

wound to produce even more ROS.[7] Therefore, combination therapy that targets both oxidative stress and bacterial infection is necessary to improve wound healing.

Currently, collaborative antioxidant and antibacterial therapies are gradually attracting more attention. Researchers have developed various systems for specific purposes, such as gels,[8] nanofiber drug carriers,[9,10] and cell carriers.[11,12] These advancements highlight the potential of synergistic approaches that combine antioxidant and antibacterial properties in addressing complex medical challenges. However, hydrogels have yet to be widely utilized as wound dressings in the biomedical field due to their suboptimal mechanical properties and inadequate adhesion.[13,14] Porous sponge scaffolds have restricted functionality and may cause skin ulceration due to their poor mechanical performance.[15] While nanosilver films possess desirable mechanical properties, breathability, and the ability to protect wounds from bacterial invasion,[16] they also have shortcomings such as insufficient space for fluids, challenging handling, and difficulties in adhering to wound beds.[17] It is of great significance to develop nanomedicine in a simple way and realize two functions at the same time to promote wound healing in patients with diabetes.

Over the past few decades, polysaccharides from traditional Chinese medicine have attracted significant attention due to their excellent and unique antioxidant activity.[18] For example, angelica polysaccharides have been shown to improve Superoxide dismutase (SOD) activity in mice,[19] codonopsis polysaccharides have been found to increase Glutathione peroxidase (GSH-Px) activity in mice,[20] and poria polysaccharides have been demonstrated to reduce Malondialdehyde (MDA) content in rats.[21] The fungus *P. sanguineus* is a versatile material widely used in biodegradation,[22] wastewater treatment,[23] and wood bleaching,[24] among other fields. Its fruiting body contains bioactive substances such as polysaccharides and enzymes.[25,26] Research by Chen has shown that extracts from P. sanguineus exhibit a therapeutic effect in relieving inflammation associated with ulcerative colitis, possibly by inhibiting apoptosis induction in Th cells and restoring the epithelial barrier.[27,28] These bioactive compounds have wide-ranging applications in the field of biomedicine. Furthermore, our study found that polysaccharides extracted from *P. sanguineus* possess excellent antioxidant capabilities. These polysaccharides effectively eliminate free radicals and alleviate cellular oxidative stress. These findings provide a significant foundation for further research and the development of therapeutic interventions utilizing *P. sanguineus* polysaccharides. However, these polysaccharides do not possess antibacterial properties and instead provide N and C sources for bacterial growth, limiting their efficacy in treating skin infections. To address this issue, modifying polysaccharides with different antibacterial materials can enhance their efficacy and expand their range of application.

Silver has been proven to be an effective bactericide, as it penetrates bacterial cell walls and membranes to cause protein denaturation and bacterial death.[29] Furthermore, smaller silver particles exhibit stronger bactericidal activity,[30] addressing the issue of bacterial resistance to antibiotics. Polysaccharides containing hydroxyl and aldehyde groups can form complexes with silver ions and reduce them to silver nanoparticles,[31] which are deposited on the polysaccharide surface via electrostatic interactions.[32] While metal particle aggregation can cause silver particles to continuously grow, the structure of polysaccharides stabilizes the particles, preventing further growth and ultimately leading to the formation of composite particles with specific shapes and sizes.[33]

Building on this foundation, this study aims to develop polysaccharide-silver nanoparticle composite particles that can promote wound healing in diabetic foot ulcers by combining antioxidant and antibacterial properties. This study aimed to develop a novel therapeutic material, PCPs, by utilizing the integrated antioxidant properties of *P. sanguineus* polysaccharides and the antibacterial functionality of silver. This research aimed to provide a new approach for treating diabetic foot ulcers and promoting wound healing.

Materials and Methods

Materials

The strain of *P. sanguineus* was purchased from the China Center for the Preservation and Management of Industrial Microbial Cultures (CICC 50181). Silver nitrate ($AgNO_3$) is obtained from Sinopharm Chemical Reagents Ltd. and other analytical grade chemicals from Sigma. In the experiments described in this article, the water used was purified using a Milli-Q water purification system (Millipore). The reagent sets utilized to quantify tissue homogenate antioxidant

markers (SOD, GSH-PX, CAT, MPO, and MDA) was procured from Nanjing Jiancheng Bioengineering Institute (Nanjing, China).

Extraction and Identification of Polysaccharides of P. Sanguineus

We modified the previous method and realized the extraction of crude polysaccharides from *P. sanguineus*.[34] After collecting the *P. sanguineus*, it was freeze-dried and ground to obtain *P. sanguineus* powder. The resulting powder was mixed with pure water at a ratio of 1:50 (w/v) and stirred at 95°C using a magnetic stirrer for 3 h. The solution is centrifuged to collect only the supernatant, which evaporates at 55°C to remove water and obtain a concentrated solution. Mix the concentrated polysaccharide with three volumes of absolute ethanol, and then precipitate the polysaccharide with ethanol at 4°C. Crude polysaccharides are purified by the Sevage[35] method. The DEAE-52 column (3 cm × 25 cm) is used to re-dissolve and purify the polysaccharides, which are then eluted at a flow rate of 1 mL/min using a high concentration of NaCl (2.5 M). The eluate was collected, dialyzed and freeze-dried to obtain purified polysaccharides.

Fourier transform infrared (FTIR, Thermo Scientific Nicolet 6700, USA) spectroscopy performed infrared spectroscopy in the 4000–400 cm^{-1} range for polysaccharide functional groups. To determine the Mw, Mn, and Mz of PCPs, high-performance gel permeation chromatography (HPGPC) was conducted using a Wyatt ELEOS System and Shodex OHpak SB-806 column with refractive index detection. The monosaccharide composition was analyzed using gas chromatography (GC, 1200, Agilent Technologies, USA). Standard chromatograms were used to determine the relative molar ratios of rhamnose, fucose, ribose, arabinose, xylose, mannose, galactose, and glucose via area normalization.

Green Synthesis of PCPs

We modified the method of Alexey Lunkov[36] to synthesize polysaccharide-based composite particles (PCPs). Firstly, the purified polysaccharide was dissolved in water to prepare a solution with a concentration of 2 mg/mL. Then, the polysaccharide solution was added to a 1 mM $AgNO_3$ aqueous solution in a volume ratio of 10:1. The mixture was stirred in a dark environment at 35°C. After 24 hours, the mixture was centrifuged at a speed of 10,000 rpm for 30 minutes using a high-speed centrifuge. After removing the supernatant, the synthesized product pentachlorophenol was further purified by washing it three times with ethanol and distilled water. Finally, the solid pentachlorophenol was obtained through freeze-drying

Characterization of PCPs

The initial formation of PCPs was observed by solution color change and UV-Vis (K7001, YOKE, China) absorption values of the solution were recorded using a UV spectrophotometer in the wavelength range of 300–600 nm. The particle size of the nanoparticles is measured in a Malvern particle analyzer (DLS, Malvern Nano-ZS 90, Malvern, UK). PCPs were deposited on a carbon-coated copper grid and dried naturally at room temperature, Silver nanoparticle size, shape, and morphology were observed by high-resolution transmission electron microscopy (TEM, H-7000, HITACHI, Japan). The crystal structure of PCP was analyzed by X-ray diffraction (XRD, D8 Advance, BRUKER, Germany), measured in the range of 10–90° 2θ. FTIR analysis was performed in the 4000–400 cm^{-1} range to scan and determine functional groups in PCPs synthesis.

Antioxidant Activity of PCPs: ABTS Determination

The Arata Badano method was employed to determine the in vitro antioxidant activity of PCPs. The sample to be measured was dissolved and diluted to different concentrations, and 50 μL of the sample to be tested was mixed with 150 μL ABTS working solution and reacted for 30 min at room temperature. Absorbance is measured at 734 nm.

The cleanup capability (%)= [1−(Ai−Aj)/A0] × 100%

Where Ai represents the absorbance value of the solution after adding the sample, Aj represents the absorbance value of the sample solution, and A0 presents the absorbance value of the ABTS+ solution.

Bacteriostatic Assay

Staphylococcus aureus (ATCC 25923) and Escherichia coli (ATCC 25922) were used in this study. The bacteria was in Luria bertain (LB) broth at 37°C until they reached the logarithmic growth phase, subsequently the concentration of the bacterial suspension was adjusted to 10^6 CFU/mL. Add the bacterial suspension (100 μL, 1×10^6 CFU/mL) to a 96-well culture plate containing PCPs. After incubation at 37°C for 12 h, the obtained bacterial suspension is smeared on LB agar plates. Then, incubate for an additional 12 h at 37°C to form observable colony units and take pictures of LB plates. Use the live/dead bacteria staining kit (Live&Dead Bacterial Staining Kit, YEASEN, China) to stain the above suspension after co-culture with PCPs.

Cytotoxic Activity of PCPs

Assess the cytotoxic activity of PCPs using MTT assay. The L929 and HaCaT cells were cultured in high-sugar DMEM medium supplemented with 10% fetal bovine serum and maintained at 37°C with 95% air and 5% CO_2. The cultured cells (100 μL and 8000 cells/well) are then seeded in 96-well plates and incubated for 24 h. After incubation, different concentrations of PCPs are added to each well and incubated for 24 h, with untreated cells used as controls. After incubation, add 10 μL MTT to each well and incubate at 37°C for 4 h. Add dimethyl sulfoxide and measure the absorbance at 490 nm using a microplate reader (1,681,130, Bio-Rad, USA).

Antioxidant Properties at the Cellular Level of PCPs

Select well-grown L929 and HaCaT cells, dilute them into 8×10^4 single-cell suspensions, and seed 100 μL in 96-well plates for 12 h. Add PCPs diluted with serum-free medium and continue the culture for 24 h. In the normal wells, add 200 μL of serum-free medium. In the control well and experimental well, add H_2O_2 dilution (concentration 500 μM) to induce for 30 minutes. After adding the DCFH-DA probe to the solution, the final concentration of the probe is 4 μM. After incubating for 20 minutes, the cells are washed three times with PBS to remove extracellular probes. Collect the cells and measure the fluorescence intensity value using a multifunctional fluorescent microplate reader (F-4600, HITACHI, Japan) under 488 pm excitation light and 525 nm emission light.

Animal Experiments

Male C57BL/6 mice (age 7 weeks, body weight 18 ± 2 g) from Jinan Pengyue Laboratory Animal Breeding Co., Ltd. (Jinan, China). All animal treatments were approved by the Ethics Committee of Weifang Medical University by the Guide for the Care and Use of Laboratory Animals published by the National Research Council (2022SDL443). The experimental protocols were conducted by the ARRIVE guidelines.

The room temperature is maintained at 23 ± 2°C, and the mice are exposed to 12 h of light daily. After the adaptation feeding period, Streptozotocin (STZ, 100 mg/kg) was rapidly injected via intraperitoneal injection for 5 consecutive days. Blood glucose levels were monitored using a glucometer by tail vein bleeding. The modeling was successful if the blood glucose level was >16.7 mM, and the mouse was considered a diabetic model.

Mice were randomly assigned to one of four groups containing 24 mice. The experimental groups included the normal control group, polysaccharide treatment group, $AgNO_3$ treatment group, and PCPs treatment group. To create wounds, after anesthetizing the mice, the hair on the back of the mice was removed, and a 6 mm punch biopsy was used to create a full-thickness excisional skin wound on the dorsal skin of the mice. Tissues of all mice were infected with 50 μL of a suspension containing 1.0×10^6 CFU/mL of *S. aureus* and *E. coli* to establish the infected experimental model. From day 3 onwards, 20 μL of normal saline, polysaccharide (30 μg/mL), $AgNO_3$ (30 μg/mL), and PCPs (30 μg/mL) were directly applied to the wound site every day. Digital cameras were used to capture daily images of the wounds to record the healing process. Image J software was used to measure and calculate the wound area. On days 6, 12, and 18 after injury, mice were euthanized, and the wound and surrounding skin were excised for analysis.

Wound Antibacterial Analysis

To study the change in the number of bacteria in infected wounds in mice, we need to count the number of bacteria in the wound during the wound healing process in mice, add normal saline (1:9, w/v) to the wound tissue sampled on days 6, 12, and 18, and grind on ice into tissue homogenate. The tissue fluid obtained after homogenization was diluted with normal saline. The tissue homogenization dilution of different gradients was plated on a solid medium for counting. The bacterial amount at the original wound was calculated according to the diluted bacterial amount.

Pathological Section

Histochemical analysis is performed on the wound tissue and the surrounding skin tissue at the wound edge to observe the healing process of the wound. The tissue sample is subjected to the following processing steps: it is first fixed in 4% paraformaldehyde, then embedded in paraffin, and cut into 6 mm-thick sections. At least 5 serial sections are obtained near the center of each wound for histological examination, which involves dewaxing, rehydration, and staining with hematoxylin-eosin (H&E). Masson's Tricolor Staining Kit is used for staining, and the sections are observed under a light microscope at a magnification of 200×.

Antioxidant Capacity Test in vivo

Following homogenization of the wound, centrifuge the sample for 20 minutes (5000 rpm, 4°C) to collect the supernatant for further analysis. The activity of SOD, GSH-PX, CAT, and MPO, as well as the content of MDA, were determined in the supernatant.

Statistical Analysis

The experimental data were averaged ± standard deviation, repeated three independent experiments, and statistically different analysis was performed by one-way ANOVA analysis and Student's *t*-test analysis data. $P<0.05$ was significantly different and was considered statistically significant.

Results and Discussion

Characterization of Polysaccharides and PCPs

In order to perform a precise analysis of the polysaccharides contained in the bacteria, we carried out GC analysis. (Figure S1), the polysaccharides of *P. sanguineus* are composed of mannose, glucuronic acid, glucose, galacturonic acid, galactose, arabinose and fucose, and the molar ratio is 1:0.7:12.98:0.14:2.35:0.001:0.39 (Table S1). The HPGPC analysis showed that the polydispersity of PCPs was 1.17, and the Mw, Mn, and Mz were 2.39×10^5, 2.05×10^5, and 7.18×10^5 Da, respectively (Table S2).

The functional groups on the surface of the polysaccharides indicate possible reducibility. Therefore, we mixed the polysaccharides with $AgNO_3$ (Figure 1). The results showed that the solution gradually changes from light yellow to dark brown (Figure S2) with the extension of time after mixing and stirring. Because silver appears tan in the solution, the color change indicates that silver ions are reduced to elemental silver by polysaccharides.[37] The corresponding UV-Vis spectral result (Figure 2A) has a distinct absorption peak at 416 nm. This is due to the absorption of nanoscale silver surface plasmon to form an absorption peak, proving that silver ions are reduced to nanoform to a higher degree.[38]

The changes in functional groups are crucial for the study of PCP synthesis. Therefore, FTIR identified the functional groups of polysaccharides responsible for reducing and stabilizing silver between 4000 cm^{-1} and 400 cm^{-1} and verified the generation of PCPs.[39] The absorption bands observed in the FTIR spectra of polysaccharides and PCPs are almost identical (Figure 2B), indicating that PCPs are synthesized and the skeleton structure of polysaccharides remains unchanged after loading PCPs. It is worth noting that the strong absorption at 3345.21 cm^{-1} indicates the tensile vibration of -OH, indicating that PCPs preferentially interact with OH through Ag-O bonds during synthesis.[40] At 1630.37 cm^{-1}, it is generated by C=O vibration.[41] A strong absorption peak appears at 1400.06 cm^{-1} due to silver ions.[42] The tensile vibration at 1078.49 cm^{-1} can be attributed to the C-O-C bond.[43] The results showed that the carboxyl and hydroxyl groups of polysaccharides participated in the synthesis and stability of PCPs.

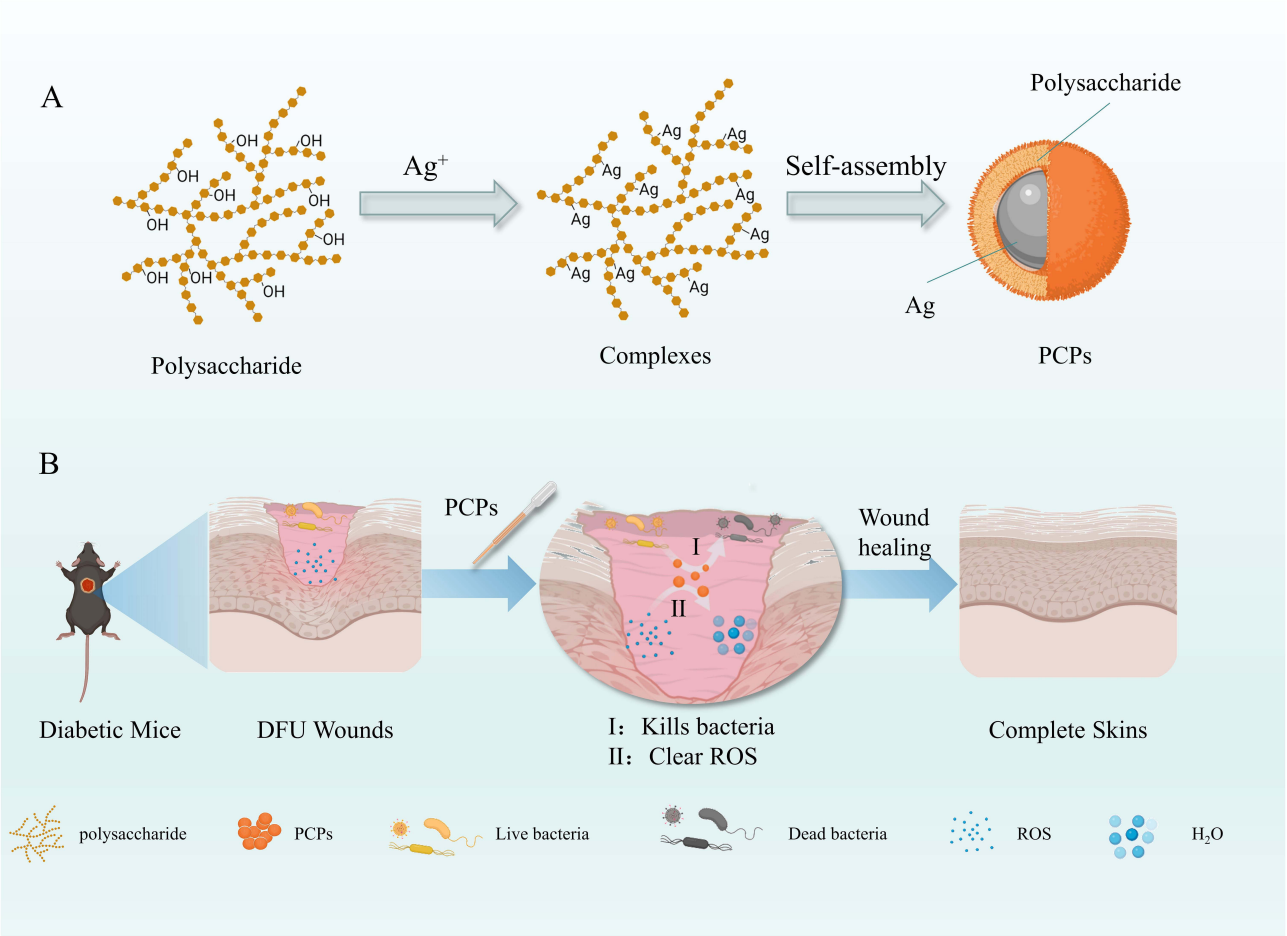

Figure 1 Schematic diagram of PCPs used to promote diabetic wound healing. PCPs that scavenge ROS and bacteria were synthesized by self-assembly of polysaccharides and silver ions (**A**), enhancing healing of diabetic wounds (**B**).

X-ray diffraction (XRD) of PCPs shows the strong signal of the PCPs by four significant diffraction peaks in the map (Figure 2C). 38.3°, 44.1°, 64.4°, and 76.6° correspond to the four faces of the silver cubic structure: (111), (200), (220), (311). The green-synthesized PCPs were found to show a consistent face-centered cubic (fcc) crystal structure, in accordance with the silver crystal structure reported in Joint Committee on Powder Diffraction Standards (JCPDS) file No. 4–0783.[44] Similar XRD patterns have been observed in other studies,[45] confirming the successful preparation of PCPs using green synthesis methods.[46] The TEM technique was used to determine the size, shape, and morphology of silver nanoparticles synthesized in situ,[47] and the resulting plot (Figure 2D) showed that the synthesized PCPs were predominantly spherical and well dispersed. In addition, the particle size recorded on the DLS instrument (Figure S3) was 57.29 ± 22.41 nm.

Cytotoxicity Test

Cytotoxicity is one of the indicators of clinical application, and we evaluated the effects of different concentrations of polysaccharides, PCPs and $AgNO_3$ on the proliferation of L929 cells (Figure 3A) and HaCaT cells (Figure S4). The growth rate of polysaccharides was greater than 100% in L929 cells and HaCaT cells in the experimental concentration range, and polysaccharides were not toxic to both cells. At a concentration of 1.95 μg/mL, $AgNO_3$ exhibited high toxicity towards HaCat cells, with a cell viability of 34.1%. Similarly, at a concentration of 7.81 μg/mL, it also showed toxicity towards L929 cells, with a cell viability of 50.84%. However, after the synthesis of PCPs, the cellular toxicity of silver was significantly improved. PCPs acted on L929 cells at a dose of 31.25 μg/mL for 24 h, with cell viability rates of 98.41% ± 6.75% and HaCaT cell survival rates above 80%. Moreover, compared to nano silver prepared using traditional

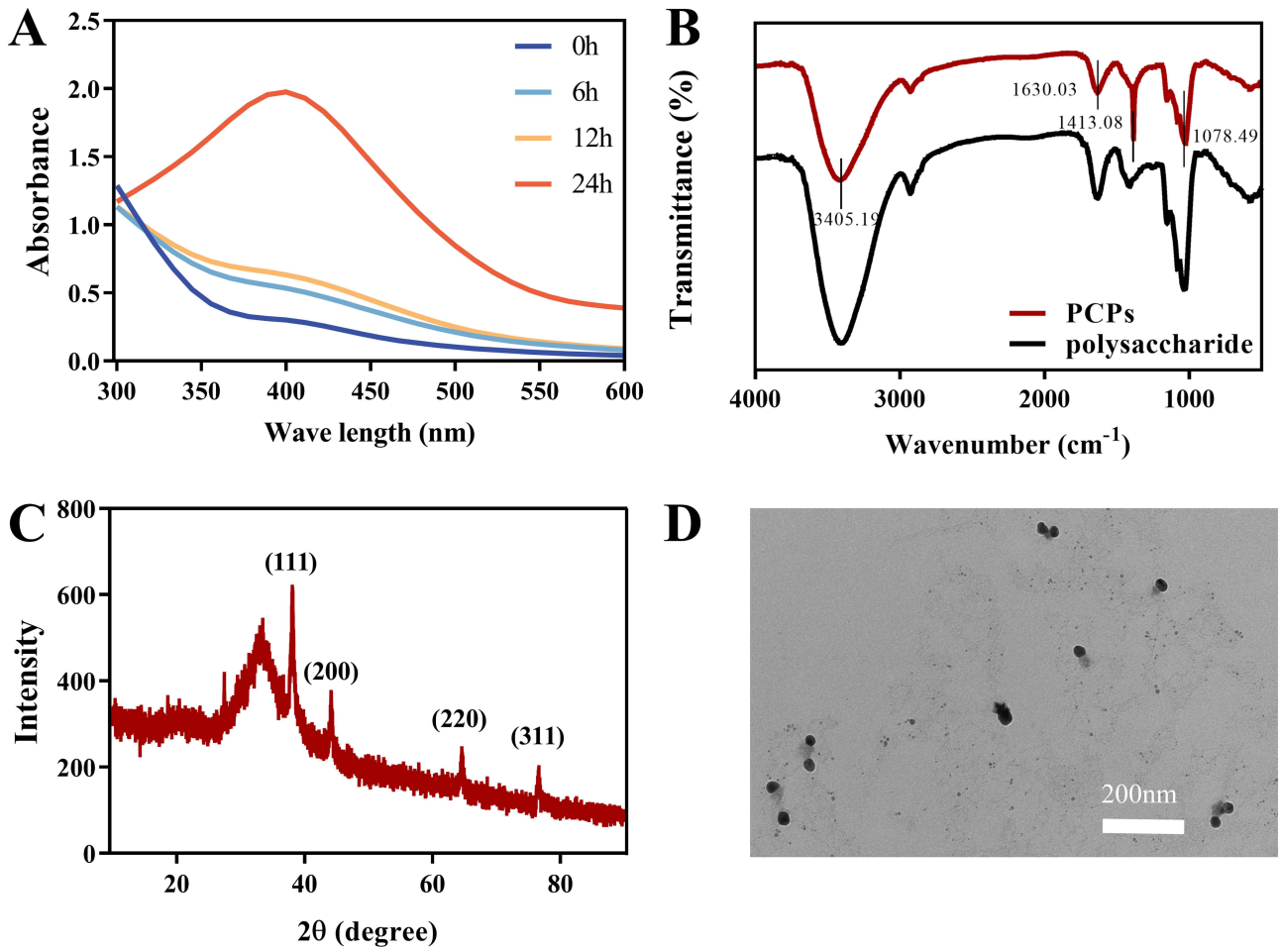

Figure 2 Characterization of the formation of PCPs. (**A**) UV spectrophotometer. (**B**) Fourier infrared detection. (**C**) XRD Inspection. (The figures were created using GraphPad Prism 9.5.1, LLC.) (**D**) Transmission electron microscopy.

physical or chemical methods, PCPs synthesized using a green synthesis approach demonstrated better improvement.[48,49] This indicates that the green synthesis method can reduce the toxic effects on cells during the preparation of nanomaterials, thereby enhancing their feasibility for biological applications.[50] These results suggest that PCPs possess low toxicity within a certain range and can be used for subsequent experiments. Considering cost and therapeutic efficacy, 30 μg/mL PCPs concentration was selected for subsequent animal experiments.

In vitro Antioxidant Activity

The in vitro antioxidant capacity of PCPs is indicated by the ability to clear $ABTS^+$ (Figure 3B). As the concentration of polysaccharides increases, the antioxidant effect of polysaccharides is better. PCPs did not lose the antioxidant properties of polysaccharides after synthesis, and the degree of anti-oxidation was positively correlated with concentration. At a 1000 μg/mL concentration, the polysaccharides exhibited a 66.69% clearance rate of $ABTS^+$. After transformation into PCPs at the same concentration, PCPs showed a clearance rate of 61.04% for $ABTS^+$. In contrast, $AgNO_3$ did not exhibit significant antioxidant capacity, with a clearance rate of only 8.94% for $ABTS^+$ at a 1000 μg/mL concentration.

These results indicate that the transformation of polysaccharides into PCPs maintains their antioxidant capacity against $ABTS^+$. PCPs demonstrated a higher clearance rate, suggesting their potential antioxidant activity. Furthermore, this study provides the first systematic validation of the antioxidant properties of *P. sanguineus* polysaccharides. The verification of the antioxidant nature of blood red polysaccharides not only fills knowledge gaps in the relevant field but

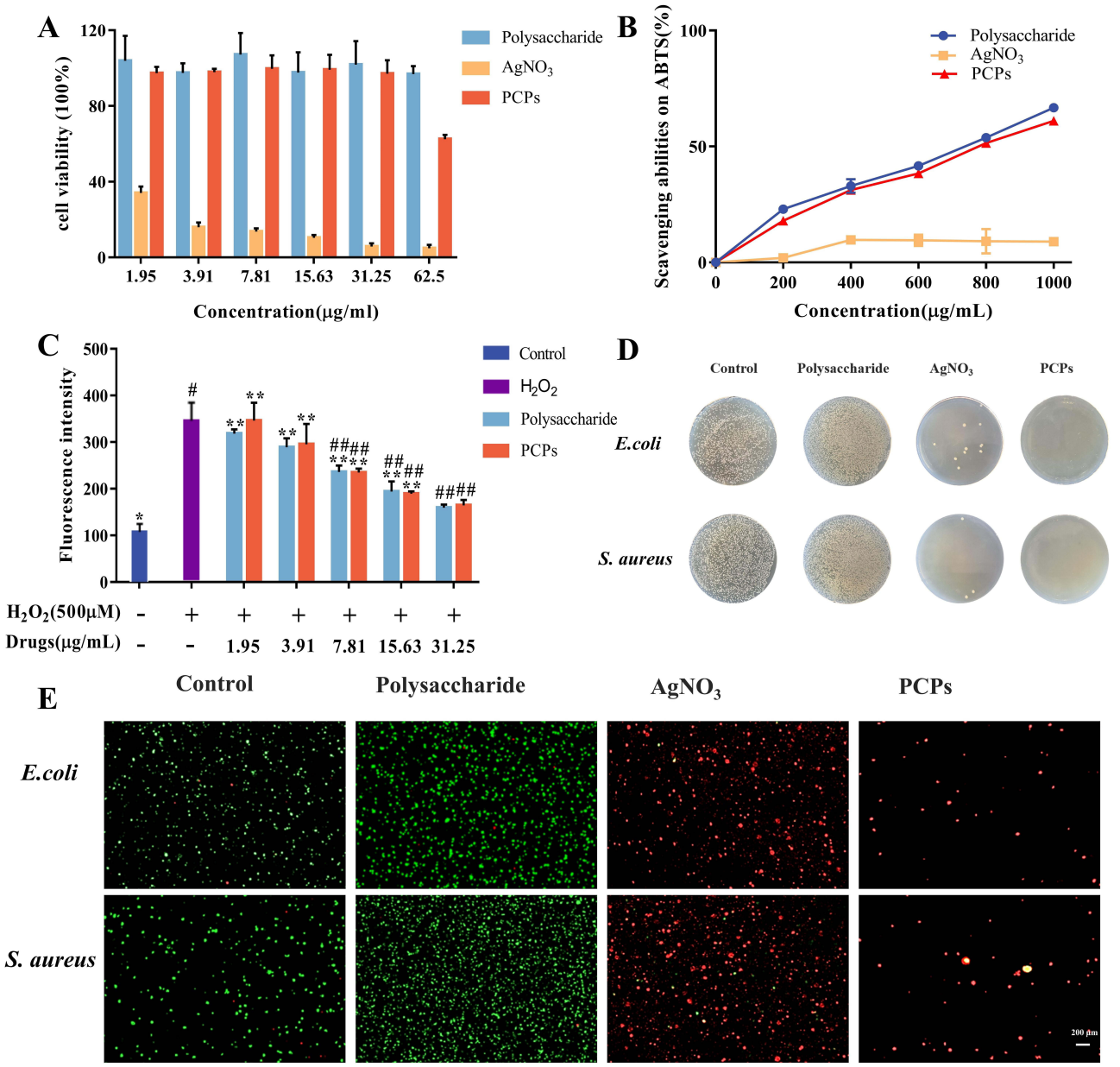

Figure 3 In vitro experiments of PCPs. (**A**) Toxicity of PCPs to L929 cells. (**B**) ABTS antioxidant test for PCPs. (**C**) PCPs for ROS scavenging assay at L929 cell level. $^{**}P < 0.01$ and $^{*}P < 0.05$ compared with normal groups (blue), $^{\#\#}P < 0.01$ and $^{\#}P < 0.05$ compared with negative control (purple), n=3. (**D**) Antibacterial tablets. (**E**) Live/dead cell staining of cells treated with the difference samples.

also provides a strong basis for further exploration of their mechanisms and the development of related antioxidant therapeutic approaches.

Cellular Antioxidant Capacity

After L929 cells (Figure 3C) and HaCaT cells (Figure S5) were induced by H_2O_2 for 30 minutes, the level of ROS in the cells was significantly elevated compared to that of normal cells. The intracellular level of L929 increased by 276.41%, and the intracellular level of HaCaT increased by 149.09%. At 31.25 μg/mL, the level of L929 intracellular ROS decreased by 54% and the level of HaCaT intracellular ROS decreased by 23.1%. PCPs also had a certain clearance ability for ROS at 31.25 μg/mL, which reduced the level of L929 intracellular ROS by 52.48% and the level of HaCaT

intracellular ROS by 21.89%. $AgNO_3$ has not been studied for antioxidant capacity due to its high cytotoxicity. Thus, PCPs exhibit a favorable ability to scavenge ROS in cells, thereby safeguarding skin cells against ROS-induced damage.

Antibacterial Effect

This study found that the original form of *P. sanguineus* polysaccharides did not exhibit significant antibacterial effects (Figure 3D). However, we observed remarkable antibacterial activity by transforming the polysaccharides into PCPs. Experimental results demonstrated that PCPs exhibited significant inhibitory effects against both *S. aureus* and *E. coli*, with a minimum inhibitory concentration (MIC) of 8 μg/mL. Importantly, the MIC of PCPs was much lower compared to other reported nanoparticles prepared using green methods.[51,52] This indicates that through the utilization of a green synthesis approach, we successfully enhanced the antibacterial efficacy of PCPs, enabling effective inhibition of target bacteria at low concentrations.

Results of live/dead cell staining 24 h after material action (Figure 3E). Live bacteria appear green under a fluorescence microscope, whereas dead bacteria appear red under a fluorescence microscope. The mortality rate of bacteria in the polysaccharide group is extremely low, and it can be considered that polysaccharides have almost no bacteriostatic effect but will also promote bacterial proliferation, which may be because polysaccharides provide C and N sources for bacterial growth. In addition, the number of dead bacteria in the $AgNO_3$ and PCPs groups increased significantly compared with the control group, proving that PCPs had Ag's antibacterial ability had the antibacterial ability of Ag and had a significant antibacterial effect.

The significant antibacterial effects observed after the transformation of polysaccharides into PCPs may be attributed to several factors. Firstly, silver nanoparticles possess excellent antibacterial activity, and their nanoscale size and surface characteristics enhance interactions with bacteria.[53] Secondly, as a carrier material, polysaccharides promote the stability of PCPs, thereby enhancing their antibacterial performance.[54] Additionally, the antibacterial mechanism of PCPs may involve the release of silver ions and their interactions with bacteria. Silver ions can interact with the cell wall and membrane surfaces of bacteria, disrupting cell structure and function, thereby inhibiting bacterial growth and proliferation.[55]

In vivo Wound Healing Studies

After different material treatments (Figure 4A), wound images were captured for each group at 0, 6, 12, and 18 days (Figure 4B). It is noteworthy that compared to the Control group, the PCPs group exhibited a significant improvement in wound healing rates at both day 6 and day 12. The PCPs group demonstrated a distinct advantage in diabetic wound healing. In contrast, the Control and Polysaccharide groups did not achieve complete healing by day 18, with wound healing rates of 93.37% and 90.9%, respectively (Figure 4C).

Bacterial quantification at the diabetic wound sites was assessed through bacterial colony counting (Figure 4D). The PCPs group showed a similar antibacterial effect in diabetic wound healing compared to the $AgNO_3$ group. Bacterial quantification at the wound sites revealed that the PCPs group had a bacterial count of 5.29 cfu/mg at day 12, significantly lower than the Control group's count of 6.68 cfu/mg *($P<0.01$)*. By day 18, the bacterial count in the PCPs group further decreased to 4.24 cfu/mg, also significantly lower than the Control group's count of 5.68 cfu/mg *($P<0.01$)*. This indicates that PCPs have a significant inhibitory effect on bacteria in diabetic wounds.

The PCPs group exhibited excellent wound healing effects in the experiment, which may be attributed to its antioxidant and antibacterial capabilities, helping reduce the risk of wound infection. Additionally, the clearance of bacteria alleviated oxidative stress at the wound site, promoting wound healing.

Histopathological Studies

Histopathological analysis of H&E-stained specimens was conducted to evaluate the healing effect (Figure 5A). On the sixth day after the wound, scabs had formed at the wound sites in all groups, and the epidermal tissue had thickened. Under the microscope, severe inflammatory responses were observed. However, the PCPs group exhibited milder

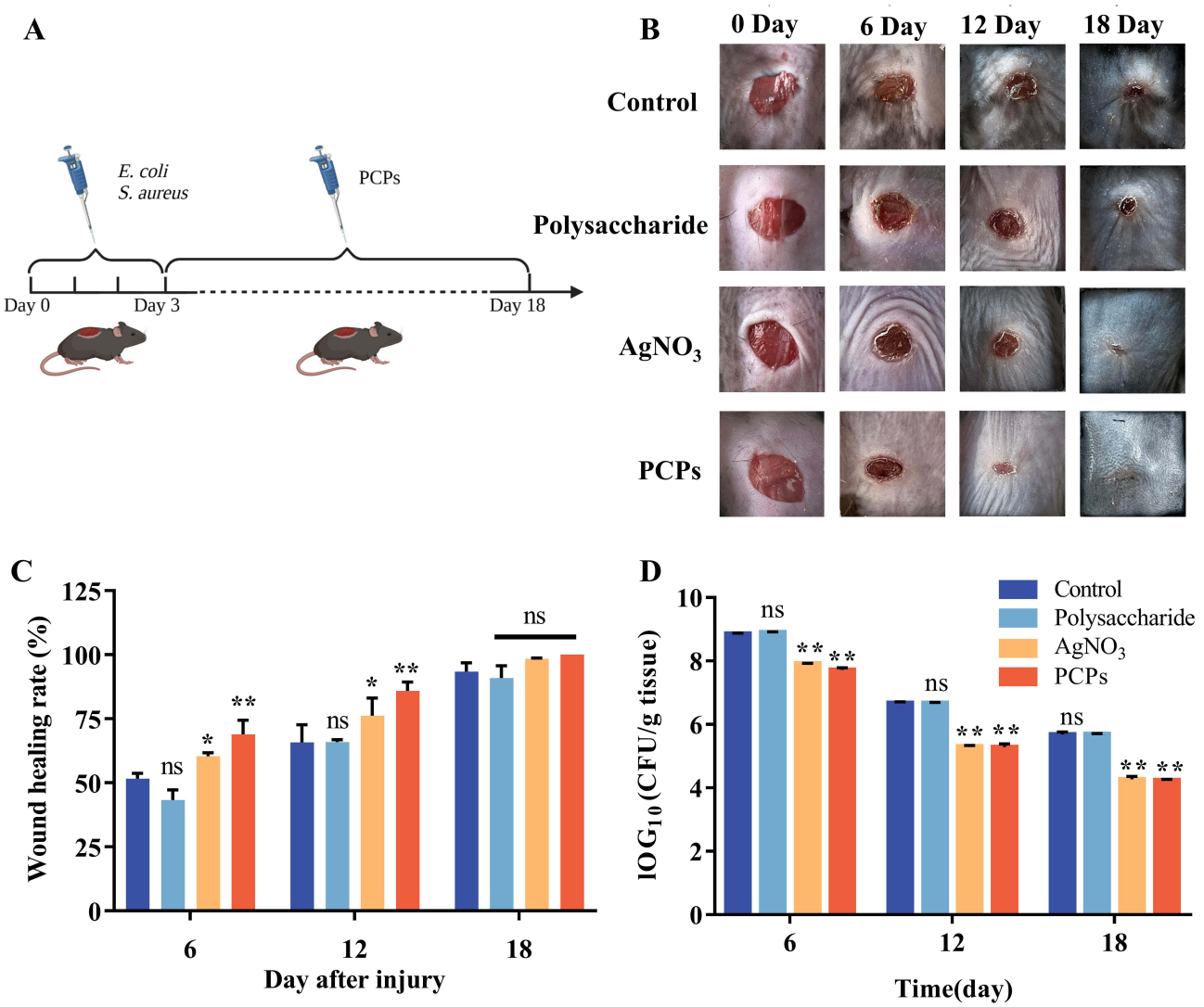

Figure 4 The promoting effect of wound healing.(**A**) Days of dosing in animal models. (**B**) Wound healing effects for different groups. (**C**) Wound healing rate. $^{**}P < 0.01$ and (*) $P < 0.05$ compared with normal groups in each day (blue), n=3. (**D**) Quantification analysis of bacterial load in the wound. $^{**}P < 0.01$ compared with normal groups in each day (purple), n=3.

inflammatory infiltrates compared to the control group. On day 12, the wound healing process was further improved in both groups, the inflammatory infiltration of the PCPs group disappeared, and the epidermis became thin and smooth.

Figure 5B shows the results of histopathological analysis of wound healing using Masson's staining. The PCPs group exhibited a higher density of collagen tissue and the same connective tissue orientation compared to the model group. Histopathological observations have shown that PCPs can shorten the inflammatory response stage time. The antioxidant capacity of PCPs works by decreasing the intensity of the inflammatory response, thereby facilitating skin wound healing.

Antioxidant Index

Peroxide dismutase (SOD) is an enzyme that is very important for fighting oxidative stress, and after skin damage, SOD converts superoxide to H_2O_2.[56] Catalase (CAT) is the most important H_2O_2 scavenging enzyme, and H_2O_2 is broken down into H_2O and oxygen molecules through CAT.[57] The experimental results showed that the PCPs group significantly increased SOD enzyme activity in diabetic mouse wounds. On day 6, the enzyme activity in the PCPs group was 12.85 U/mg, significantly higher than the Control group's activity of 9.83 U/mg. At day 12, the PCPs group exhibited an

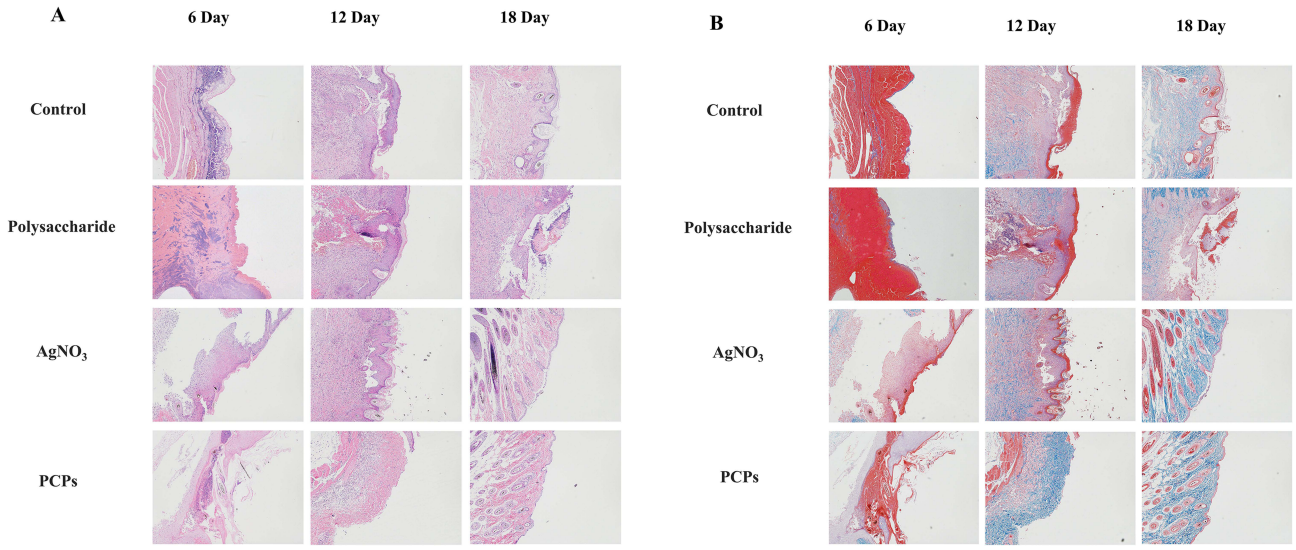

Figure 5 Pathological section. Skin samples were obtained on days 6, 12, and 18 for staining with H&E (**A**)and Masson (**B**).

enzyme activity of 19.35 U/mg, significantly higher than the Control group's activity of 13.81 U/mg (Figure 6A). During the early stages of wound healing, this could be attributed to the PCPs' ability to effectively eliminate excessive ROS and inhibit bacteria that stimulate ROS production. Consequently, the consumption of SOD enzyme was reduced, resulting in higher SOD enzyme activity in the tissues.

The CAT enzyme activity in the PCPs group remained at a high level throughout the entire wound healing period, indicating that the PCPs group exhibited sustained and elevated CAT enzyme activity (Figure 6B). This suggests that the low H_2O_2 content at the wound site resulted in minimal CAT enzyme depletion and, consequently, high enzyme activity in the tissues.

Glutathione peroxidase (GSH-Px) can convert harmful peroxides in cells into safe hydroxyl compounds and promote the decomposition of H_2O_2.[58] Still, PCPs have no significant effect on this enzyme in the early stage (Figure 6C).

In the early stages of skin damage, phagocytes myeloperoxidase (MPO) forms hypochlorous acid (HOCl) in neutrophils by H_2O_2 and chloride due to the aggregation of neutrophils.[59] At the same time, it also reflects the level of inflammation in the wound. At day 6, the PCPs group exhibited a content of 8.06 U/mg, significantly lower than the Control group's content of 11 U/mg. On day 12, the PCPs group had a content of 5.77 U/mg, which was noticeably lower than the Control group's content of 7.98 U/mg. By day 18, the PCPs group had a content of 2.87 U/mg, showing a significant difference from the Control group (Figure 6D). Due to its antibacterial properties, PCPs can reduce bacterial proliferation at the wound site, resulting in reduced neutrophil aggregation and lower MPO content. The changes in MPO content during the wound healing process corresponded to the histological findings from H&E staining, confirming that PCPs reduced inflammatory infiltration at the wound site.

Excess SOD leads to lipid peroxidation, and glutaraldehyde (MDA), as the end product of lipid peroxidation, can indirectly reflect the level of tissue oxidative damage.[60] At day 6, the PCPs group exhibited a content of 11.74 U/mg, significantly lower than the Control group's content of 14.19 U/mg. On day 12, the PCPs group had a content of 7.91 U/mg, which was noticeably lower than the Control group's content of 10.34 U/mg. By day 18, the PCPs group had a content of 2.98 U/mg, showing a significant difference from the Control group (Figure 6E). Throughout the entire wound healing process, the levels of MDA indicated the extent of oxidative stress at the wound site, and MDA content was inversely proportional to wound healing capacity. PCPs prevented lipid peroxidation by alleviating oxidative stress at the wound site, resulting in lower MDA content.

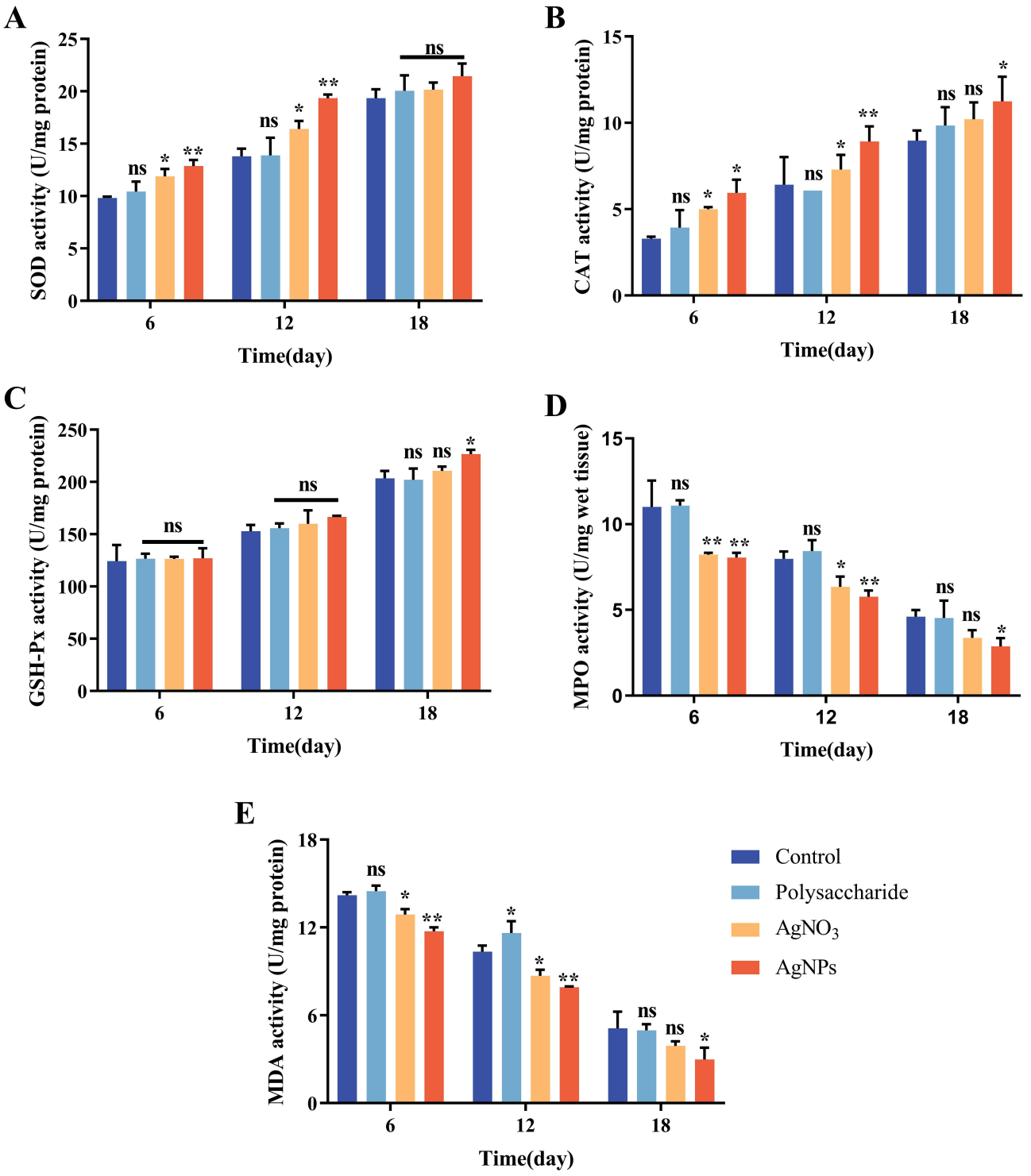

Figure 6 Antioxidant index detection. SOD (**A**), CAT (**B**), GSH-Px (**C**), MPO (**D**), MDA (**E**), **P < 0.01 and *P < 0.05 compared with normal groups in each day (blue), n = 3.

Conclusion

In this study, we investigated the polysaccharides isolated from *P. sanguineus* and validated their antioxidant properties for the first time. Through a green synthesis method, we successfully synthesized PCPs. Biological activity experiments demonstrated that PCPs exhibited no cytotoxicity to HaCat and L929 cells within a certain concentration range. Antibacterial assays revealed strong antibacterial activity of PCPs against Escherichia coli and Staphylococcus aureus,

with a MIC of 8 μg/mL. In vitro and cellular level experiments demonstrated that the synthesized PCPs retained the antioxidant capability of the polysaccharides. In vivo experiments showed that PCPs promoted healing diabetic ulcer wounds through antibacterial effects and enhancement of SOD and CAT activities.

These findings provide a new avenue for the application of polysaccharides from *P. sanguineus* and highlight their potential prospects in wound healing. Additionally, the excellent antibacterial properties exhibited by PCPs offer a new strategy for the treatment of chronic infected wounds. However, the toxicity of PCPs limits the overall drug concentration, so further research is needed on reducing the toxicity of high-concentration drugs.

Acknowledgments

This work was supported by the Natural Science Foundation of Shandong Province Project (ZR2022MH152, ZR2022QC087) and Youth Innovative Team Development Plan of Universities in Shandong Province (2019KJM003). Thanks to "Innovation Team of Precision Drug Delivery and Diagnosis and Treatment Application" of Introduction and Education Program for Young Talents in Shandong Colleges and Universities.

Disclosure

The authors report no conflicts of interest in this work.

References

1. Perez-Favila A, Martinez-Fierro ML, Rodriguez-Lazalde JG, et al. Current therapeutic strategies in diabetic foot ulcers. *Medicina*. 2019;55(11):714. doi:10.3390/medicina55110714
2. Chang M, Nguyen TT. Strategy for treatment of infected diabetic foot ulcers. *Acc Chem Res*. 2021;54(5):1080–1093. doi:10.1021/acs.accounts.0c00864
3. Jiang QW, Kaili D, Freeman J, et al. Diabetes inhibits corneal epithelial cell migration and tight junction formation in mice and human via increasing ROS and impairing Akt signaling. *Acta Pharmacol Sin*. 2019;40(9):1205–1211. doi:10.1038/s41401-019-0223-y
4. Zhao H, Huang J, Li Y, et al. ROS-scavenging hydrogel to promote healing of bacteria infected diabetic wounds. *Biomaterials*. 2020;258:120286. doi:10.1016/j.biomaterials.2020.120286
5. Kalan LR, Meisel JS, Loesche MA, et al. Strain- and species-level variation in the microbiome of diabetic wounds is associated with clinical outcomes and therapeutic efficacy. *Cell Host Microbe*. 2019;25(5):641–655. doi:10.1016/j.chom.2019.03.006
6. Zhou L, Zheng H, Liu Z, et al. Conductive antibacterial hemostatic multifunctional scaffolds based on Ti(3)C(2)T(x) MXene nanosheets for promoting multidrug-resistant bacteria-infected wound healing. *ACS Nano*. 2021;15(2):2468–2480. doi:10.1021/acsnano.0c06287
7. Ouyang J, Ji X, Zhang X, et al. In situ sprayed NIR-responsive, analgesic black phosphorus-based gel for diabetic ulcer treatment. *Proc Natl Acad Sci U S A*. 2020;117(46):28667–28677. doi:10.1073/pnas.2016268117
8. Kumar M, Keshwania P, Chopra S, et al. Therapeutic potential of nanocarrier-mediated delivery of phytoconstituents for wound healing: their current status and future perspective. *AAPS Pharm Sci Tech*. 2023;24(6):155. doi:10.1208/s12249-023-02616-6
9. Ullah S, Hussain Z, Ullah I, et al. Mussel bioinspired, silver-coated and insulin-loaded mesoporous polydopamine nanoparticles reinforced hyaluronate-based fibrous hydrogel for potential diabetic wound healing. *Int J Biol Macromol*. 2023;247:125738. doi:10.1016/j.ijbiomac.2023.125738
10. Kumar M, Hilles AR, Ge Y, et al. A review on polysaccharides mediated electrospun nanofibers for diabetic wound healing: their current status with regulatory perspective. *Int J Biol Macromol*. 2023;234:123696. doi:10.1016/j.ijbiomac.2023.123696
11. Lemarchand M, Thouin K, De Serres-Bérard T, et al. In vitro glycation of a tissue-engineered wound healing model to mimic diabetic ulcers. *Biotechnol Bioeng*. 2023;120(6):1657–1666. doi:10.1002/bit.28359
12. Xu Y, Wu X, Zhang X, et al. Living microneedle patch with adipose-derived stem cells embedding for diabetic ulcer healing. *Adv Funct Mater*. 2022;33(1):2209986. doi:10.1002/adfm.202209986
13. Ullah S, Chen X. Fabrication, applications and challenges of natural biomaterials in tissue engineering. *Applied Materials Today*. 2020;20:100656. doi:10.1016/j.apmt.2020.100656
14. Mir M, Ali MN, Barakullah A, et al. Synthetic polymeric biomaterials for wound healing: a review. *Prog Biomater*. 2018;7(1):1–21. doi:10.1007/s40204-018-0083-4
15. Graca MFP, Miguel SP, Cabral CSD, et al. Hyaluronic acid-Based wound dressings: a review. *Carbohydr Polym*. 2020;241:116364. doi:10.1016/j.carbpol.2020.116364
16. Homaeigohar S, Boccaccini AR. Antibacterial biohybrid nanofibers for wound dressings. *Acta Biomater*. 2020;107:25–49. doi:10.1016/j.actbio.2020.02.022
17. Kamoun EA, Kenawy ES, Chen X. A review on polymeric hydrogel membranes for wound dressing applications: PVA-based hydrogel dressings. *J Adv Res*. 2017;8(3):217–233. doi:10.1016/j.jare.2017.01.005
18. Zeng P, Li J, Chen Y, et al. The structures and biological functions of polysaccharides from traditional Chinese herbs. *Prog Mol Biol Transl Sci*. 2019;163:423–444.
19. Ai S, Fan X, Fan L, et al. Extraction and chemical characterization of Angelica sinensis polysaccharides and its antioxidant activity. *Carbohydr Polym*. 2013;94(2):731–736. doi:10.1016/j.carbpol.2013.02.007
20. Gao SM, Liu JS, Wang M, et al. Traditional uses, phytochemistry, pharmacology and toxicology of Codonopsis: a review. *J Ethnopharmacol*. 2018;219:50–70. doi:10.1016/j.jep.2018.02.039

21. Wang H, Mukerabigwi JF, Zhang Y, et al. *In vivo* immunological activity of carboxymethylated-sulfated (1-->3)-beta-D-glucan from sclerotium of Poria cocos. *Int J Biol Macromol*. 2015;79:511–517. doi:10.1016/j.ijbiomac.2015.05.020
22. Zhao J, Zeng S, Xia Y, et al. Expression of a thermotolerant laccase from Pycnoporus sanguineus in Trichoderma reesei and its application in the degradation of bisphenol A. *J Biosci Bioeng*. 2018;125(4):371–376. doi:10.1016/j.jbiosc.2017.11.010
23. Wesenberg D, Kyriakides I, Agathos SN. White-rot fungi and their enzymes for the treatment of industrial dye effluents. *Biotechnol Adv*. 2003;22 (1–2):161–187. doi:10.1016/j.biotechadv.2003.08.011
24. Zimbardi AL, Camargo PF, Carli S, et al. A high redox potential laccase from pycnoporus sanguineus RP15: potential application for dye decolorization. *Int J Mol Sci*. 2016;17(5):672. doi:10.3390/ijms17050672
25. Falkoski DL, Guimaraes VM, De Almeida MN, et al. Characterization of cellulolytic extract from Pycnoporus sanguineus PF-2 and its application in biomass saccharification. *Appl Biochem Biotechnol*. 2012;166(6):1586–1603. doi:10.1007/s12010-012-9565-3
26. Quiroga EN, Sgariglia MA, Molina CF, et al. Purification and characterization of an exo-polygalacturonase from Pycnoporus sanguineus. *Mycol Res*. 2009;113(Pt 12):1404–1410. doi:10.1016/j.mycres.2009.09.007
27. Chen X, Li M, Li D, et al. Ethanol extract of Pycnoporus sanguineus relieves the dextran sulfate sodium-induced experimental colitis by suppressing helper T cell-mediated inflammation via apoptosis induction. *Bio Pharmaco*. 2020;127:110212. doi:10.1016/j.biopha.2020.110212
28. Jaszek M, Osinska-Jaroszuk M, Sulej J, et al. Stimulation of the antioxidative and antimicrobial potential of the blood red bracket mushroom pycnoporus sanguineus (Higher Basidiomycetes). *Int J Med Mushrooms*. 2015;17(8):701–712. doi:10.1615/IntJMedMushrooms.v17.i8.10
29. Chang -T-T, Chao C-H, Lu M-K. Enhanced biomass production of Pycnoporus sanguineus and alterations in the physiochemical properties of its polysaccharides. *Carbohydr Polym*. 2011;83(2):796–801. doi:10.1016/j.carbpol.2010.08.055
30. Soliman MKY, Salem SS, Abu-Elghait M, et al. Biosynthesis of silver and gold nanoparticles and their efficacy towards antibacterial, antibiofilm, cytotoxicity, and antioxidant activities. *Appl Biochem Biotechnol*. 2023;195(2):1158–1183. doi:10.1007/s12010-022-04199-7
31. Cai Z, Dai Q, Guo Y, et al. Glycyrrhiza polysaccharide-mediated synthesis of silver nanoparticles and their use for the preparation of nanocomposite curdlan antibacterial film. *Int J Biol Macromol*. 2019;141:422–430. doi:10.1016/j.ijbiomac.2019.09.018
32. Shahid Ul I, Butola BS, Kumar A. Green chemistry based in-situ synthesis of silver nanoparticles for multifunctional finishing of chitosan polysaccharide modified cellulosic textile substrate. *Int J Biol Macromol*. 2020;152:1135–1145. doi:10.1016/j.ijbiomac.2019.10.202
33. Hidayat MI, Adlim M, Maulana I, et al. Green synthesis of chitosan-stabilized silver-colloidal nanoparticles immobilized on white-silica-gel beads and the antibacterial activities in a simulated-air-filter. *Arab J Chem*. 2022;15(2):103596. doi:10.1016/j.arabjc.2021.103596
34. Luo L, Wang Y, Zhang S, et al. Preparation and characterization of selenium-rich polysaccharide from Phellinus igniarius and its effects on wound healing. *Carbohydr Polym*. 2021;264:117982. doi:10.1016/j.carbpol.2021.117982
35. Miao S, Mao X, Pei R, et al. Antitumor activity of polysaccharides from Lepista sordida against laryngocarcinoma *in vitro* and in vivo. *Int J Biol Macromol*. 2013;60:235–240. doi:10.1016/j.ijbiomac.2013.05.033
36. Lunkov A, Shagdarova B, Konovalova M, et al. Synthesis of silver nanoparticles using gallic acid-conjugated chitosan derivatives. *Carbohydr Polym*. 2020;234:115916. doi:10.1016/j.carbpol.2020.115916
37. Wang D, Xue B, Wang L, et al. Fungus-mediated green synthesis of nano-silver using Aspergillus sydowii and its antifungal/antiproliferative activities. *Sci Rep*. 2021;11(1):10356. doi:10.1038/s41598-021-89854-5
38. Kamradgi S, Babanagare S, Gunagambhire VM. Characterization of Talaromyces islandicus-mediated silver nanoparticles and evaluation of their antibacterial and anticancer potential. *Microsc Res Tech*. 2022;85(5):1825–1836. doi:10.1002/jemt.24044
39. Mohamed TA. Raman, Infrared & NMR spectroscopy: advances in structural, conformational and environmental analysis. *Comb Chem High Throughput Screen*. 2020;7(23):566–567.
40. Liang XX, Gao YY, Pan Y, et al. Purification, chemical characterization and antioxidant activities of polysaccharides isolated from Mycena dendrobii. *Carbohydr Polym*. 2019;203:45–51. doi:10.1016/j.carbpol.2018.09.046
41. Martinez-Felipe A, Brebner F, Zaton D, et al. Molecular recognition via hydrogen bonding in supramolecular complexes: a fourier transform infrared spectroscopy study. *Molecules*. 2018;23(9):2278. doi:10.3390/molecules23092278
42. Coates J. *Interpretation of Infrared Spectra, a Practical Approach*. John Wiley & Sons;2006.
43. Wang Y, Li Y, Li S, et al. Extracellular polysaccharides of endophytic fungus Alternaria tenuissima F1 from Angelica sinensis: production conditions, purification, and antioxidant properties. *Int J Biol Macromol*. 2019;133:172–183. doi:10.1016/j.ijbiomac.2019.03.246
44. Daglioglu Y, Ozturk BY, Khatami M. Apoptotic, cytotoxic, antioxidant, and antibacterial activities of biosynthesized silver nanoparticles from nettle leaf. *Microsc Res Tech*. 2023;86(6):669–685. doi:10.1002/jemt.24306
45. Deeba F, Parveen S, Rashid Z, et al. Green Synthesis and Evaluation of *Lepidium didymum*-mediated Silver Nanoparticles for *in vitro* antibacterial activity and wound healing in the animal model. *J Oleo Sci*. 2023;72(4):429–439. doi:10.5650/jos.ess22380
46. Gesswein H, Stuble P, Weber D, et al. A multipurpose laboratory diffractometer for operando powder X-ray diffraction investigations of energy materials. *J Appl Crystallogr*. 2022;55(Pt 3):503–514. doi:10.1107/S1600576722003089
47. Egerton RF. TEM-EELS: a personal perspective. *Ultramicroscopy*. 2012;119:24–32. doi:10.1016/j.ultramic.2011.11.008
48. Grzesiakowska A, Kasprowicz MJ, Kuchta-Gladysz M, et al. Genotoxicity of physical silver nanoparticles, produced by the HVAD method, for Chinchilla lanigera genome. *Sci Rep*. 2021;11(1):18473. doi:10.1038/s41598-021-97926-9
49. Agarwal A, Weis TL, Schurr MJ, et al. Surfaces modified with nanometer-thick silver-impregnated polymeric films that kill bacteria but support growth of mammalian cells. *Biomaterials*. 2010;31(4):680–690. doi:10.1016/j.biomaterials.2009.09.092
50. Alsareii SA, Manaa Alamri A, Alasmari MY, et al. Synthesis and characterization of silver nanoparticles from rhizophora apiculata and studies on their wound healing, antioxidant, anti-inflammatory, and cytotoxic activity. *Molecules*. 2022;27(19):6036. doi:10.3390/molecules27196306
51. Zuhrotun A, Oktaviani DJ, Hasanah AN. Biosynthesis of gold and silver nanoparticles using phytochemical compounds. *Molecules*. 2023;28 (7):3240. doi:10.3390/molecules28073240
52. Keskin M, Kaya G, Bayram S, et al. Green synthesis, characterization, antioxidant, antibacterial and enzyme inhibition effects of chestnut (Castanea sativa) honey-mediated silver nanoparticles. *Molecules*. 2023;28(6):2762. doi:10.3390/molecules28062762
53. Luzala MM, Muanga CK, Kyana J, et al. A critical review of the antimicrobial and antibiofilm activities of green-synthesized plant-based metallic nanoparticles. *Nanomaterials*. 2022;12(11):1841. doi:10.3390/nano12111841
54. Choudhury H, Pandey M, Lim YQ, et al. Silver nanoparticles: advanced and promising technology in diabetic wound therapy. *Mater Sci Eng C Mater Biol Appl*. 2020;112:110925. doi:10.1016/j.msec.2020.110925

55. Wang C, Zhu S, Liang Y, et al. Flexible free-standing antibacterial nanoporous Ag ribbon. *J Colloid Interface Sci*. 2023;645:287–296. doi:10.1016/j.jcis.2023.04.153
56. Zhang W, Hu S, Yin JJ, et al. Prussian blue nanoparticles as multienzyme mimetics and reactive oxygen species scavengers. *J Am Chem Soc*. 2016;138(18):5860–5865. doi:10.1021/jacs.5b12070
57. Zhang Y, Jin Y, Cui H, et al. Nanozyme-based catalytic theranostics. *RSC Adv*. 2019;10(1):10–20. doi:10.1039/C9RA09021E
58. Rushworth GF, Megson IL. Existing and potential therapeutic uses for N-acetylcysteine: the need for conversion to intracellular glutathione for antioxidant benefits. *Pharmacol Ther*. 2014;141(2):150–159. doi:10.1016/j.pharmthera.2013.09.006
59. Aratani Y. Myeloperoxidase: its role for host defense, inflammation, and neutrophil function. *Arch Biochem Biophys*. 2018;640:47–52. doi:10.1016/j.abb.2018.01.004
60. Tsikas D. Assessment of lipid peroxidation by measuring malondialdehyde (MDA) and relatives in biological samples: analytical and biological challenges. *Anal Biochem*. 2017;524:13–30. doi:10.1016/j.ab.2016.10.021

International Journal of Nanomedicine Dovepress

Publish your work in this journal

The International Journal of Nanomedicine is an international, peer-reviewed journal focusing on the application of nanotechnology in diagnostics, therapeutics, and drug delivery systems throughout the biomedical field. This journal is indexed on PubMed Central, MedLine, CAS, SciSearch®, Current Contents®/Clinical Medicine, Journal Citation Reports/Science Edition, EMBase, Scopus and the Elsevier Bibliographic databases. The manuscript management system is completely online and includes a very quick and fair peer-review system, which is all easy to use. Visit http://www.dovepress.com/testimonials.php to read real quotes from published authors.

Submit your manuscript here: https://www.dovepress.com/international-journal-of-nanomedicine-journal